Journal of Radiation and Nuclear Applications
An International Journal

http://dx.doi.org/10.18576/jrna/100203

Developed Austenitic Stainless Steel Fuel Cladding for a Fast Nuclear Reactor

Sara E. Saleh [1*], *H. A. Saudi* [1], *M. K. Elfawakhry*[2], *S. M. El-Minyawi* [1], *M.M. Eissa* [2]

[1]Physics Department, Faculty of Science, Al-Azhar University, Girl's branch, Cairo, Egypt.
[2]Steel Technology Department, Central Metallurgical Research and Development Institute (CMRDI), Helwan, Egypt.

Received: 02 Jan. 2025, Revised: 09 Mar. 2025, Accepted: 11 Mar. 2025.
Published online: 1 May 2025.

Abstract: In the present study, a series of austenitic stainless-steel alloys were developed for fuel cladding in fast breeder reactors. Standard austenitic stainless steel SS304L and SS316L were prepared and studied as a reference sample. The other samples were prepared by interchanging the molybdenum in standard SS316L with tungsten and adding titanium to the standard samples. The thermodynamic calculation was established using the JMatPro database to identify the phases that can be formed in the prepared samples. The microstructure properties of the present stainless-steel alloys were investigated using an optical microscope, Mainly, an austenite phase was observed for the prepared stainless-steel alloys. The mechanical properties of the prepared alloys were studied using Vickers hardness and tensile tests at room temperature which indicated that the modified austenitic stainless steel samples containing tungsten and titanium have preferable properties, higher hardness, yield strength, and ultimate tensile strength, among all other investigated samples in comparison with the standard SS316L and SS304L. Monte Carlo simulations program MNCP5 were used to determine the critical gamma radiation attenuation characteristics, particularly linear attenuation coefficients, mass attenuation coefficients, and half-value layer of the investigated stainless-steel alloys. Also, MNCP5 was used to calculate the Total neutron cross-section, absorption neutron cross-section, and mean free path at a high neutron energy range from about (0.5 to 11MeV).

Keywords: Stainless steel alloys, Fuel cladding, Microstructure, Mechanical properties, Neutron cross-section.

1 Introduction

Nuclear energy provides more than 10% of electrical power internationally, and the increasing engagement of nuclear energy is essential to meet the rapid worldwide increase in energy demand. A paramount challenge in the development of advanced nuclear reactors is the discovery of advanced structural materials that can endure extreme environments, such as severe neutron irradiation damage at high temperatures [1]. Nuclear materials for advanced nuclear plants must be able to operate under demanding exposure conditions such as temperature, radiation, and corrosive media. Stainless steels are robust materials with good corrosion resistance credit to the thin oxide layer formed by chromium [2,3]. The material must also have suitable thermal properties because recycle reactors will operate at elevated temperatures, the materials must have good elevated-temperature mechanical properties, including creep resistance, long-term stability, and compatibility with the reactor coolant [4]. The cladding and duct materials in a fast reactor are exposed to an extremely challenging environment including neutron irradiation, liquid metal corrosion, and fuel interaction combined with significant stresses. The specific environment depends on the component location. Typical coolant temperatures in the reactor core are 400–560°C but coolant temperature at the inlet can range from 250°C to 400°C, depending on reactor design. Steels are utilized extensively for structural components in many Reactor designs and other high-temperature applications [5]. Cladding tubes are a vital part of a nuclear reactor because they not only provide an enclosure to the highly radioactive fuel but also remain in direct contact with the coolant during reactor operation making it vulnerable to corrosion [6]. There are many requirements for all nuclear reactor structural materials, regardless of the exact reactor design or purpose. The material must be available, affordable, and have good fabrication and joining properties. Good neutronics (low neutron absorption) are important, especially for clad and duct applications. Stainless steel alloys are the common structural materials in-core and out-of-core components of nuclear power plants. Their high resistance to degradation by irradiation is important for nuclear applications [7,8].

Austenitic stainless steels in the 300 series were initially employed because of their good long-term mechanical

*Corresponding author e-mail: Sara E. Saleh (sarael-sayed.5919@azhar.edu.eg)

properties at high temperatures, their excellent chemical compatibility with sodium, and their stability when in contact with uranium and plutonium-bearing metallic, oxide, carbide, nitride, and inert matrix fuels [9]. Austenitic stainless steels, particularly AISI316 stainless steel, are used for radiation shielding in a variety of applications, most commonly in nuclear reactors as structural shielding materials at reactor core heat transport systems and in neutron moderator systems [10]. Accordingly, alloy D9 with appropriate modifications of Ni and Cr content with Ti additions has been developed for use as the core structural material for the upcoming Prototype Fast Breeder Reactor (PFBR) [11]. The titanium-modified steels exhibited greatly improved swelling resistance under breeder reactor conditions [12] and consequently, have become a prime candidate for structural applications. In the cold-worked Ti-modified austenitic stainless steels, the formation of fine stable precipitates of TiC termed secondary precipitates has been reported to enhance the resistance against void swelling, helium embrittlement, and in-pile creep during irradiation. Tungsten (W) is usually added to steels as strong ferrite former to improve their mechanical properties. Increasing the steel hardenability and yield strength, which was accompanied by decreasing elongation and Charpy impact energy were observed in some steel alloys as a result of adding W [13,14]. Tungsten addition was found to produce a larger carbide volume than the other alloying elements at the same C-content [15]. The consequence is the precipitation of fine or very fine carbides distributed in the steel matrix. Complex carbides are capable of retaining a finer-grained steel microstructure by retarding the grain growth during the heat treatment process. Previous results showed that, in the solution annealed condition, tungsten additions to super duplex stainless steels had a marked positive effect on pitting and crevice corrosion resistance [16]. Tungsten has also been used as a substitution for Mo in duplex stainless steels to improve corrosion resistance and prevent sigma phase precipitations during the welding thermal cycle [17].

The objective of the present work is to develop austenitic steel alloy with high mechanical properties, and good nuclear properties to be used as a fuel cladding in fast breeder reactors. Two developed alloys are based on substituting tungsten at the expense of molybdenum either by partial or complete replacement in the SS316L austenitic stainless steel, and the other two alloys are developed by modification of Cr, Ni, and micro-alloyed with titanium in standards SS316L and SS304L.

2 Experimental Section

2.1 Samples preparations

A series of austenitic stainless-steel alloys have been prepared by replacing the molybdenum with tungsten and titanium in standard stainless steel SS316L and SS304L. Sample preparations were carried out using a medium frequency induction furnace including 30 kg. Six melts were carried out. The chemical compositions of the samples that were prepared are given in Table 1 in which molybdenum was partially replaced by tungsten and titanium. The ingots of produced steel were forged at temperatures from 1000 to 1100 into square cross-section rods of 30 mm. Samples were subjected to heat treatment at 1100oC for about 1 hour, followed by water quenching. The samples were collected from rods by using an electric discharge machine (EDM). There they were subjected to microstructure observation, tensile test, and hardness.

2.2 Microstructure Examination

The metallographic examinations were carried out using cylindrical specimens cut out from the produced solution-treated steels. The specimen's surface is ground on 400, 800, 1200, and 2000-grade paper and polished on alumina paste. The microstructure is observed using an Olympus light microscope after electrochemical etching (100ml HCL, 33ml HNO3, and a few drops of H2SO4).

2.3 Mechanical Properties

Vickers hardness was measured using a Microhardness Tester FM-800e machine on polished specimens at room temperature with a 25 g load for 10 seconds. The average values of Vickers hardness were recorded for every five readings. The tensile test is carried out with a 300 kN Shenzhen Wance Testing Machine at room temperature with a constant crosshead velocity of 1 mm/min. Round tensile specimens are machined according to the specification of the ASTM E8 - 16b of 6 mm diameter and 32 mm gauge length. Ultimate tensile strength, 0.5% proof stress, and elongation to fracture were estimated throughout the tensile test. Two specimens were used for each steel and the average of them was estimated.

2.4 Density and Molar Volume Measurements

The densities of the prepared samples were measured by the displacement method using Toluene as an immersion liquid**.** The measured densities were obtained by applying the relation:

$$\boldsymbol{\rho_{sample}} = \frac{\boldsymbol{W_{air}}}{\boldsymbol{W_{air}-W_{liquid}}} \times \boldsymbol{\rho_{liquid}} \quad (1)$$

Where, W_{air}, W_{liquid} and $\boldsymbol{\rho}_{sample}$ is the weight and density of the sample respectively, ρ_{liquid}=0.8635g/cm^3. While, the theoretical density was calculated by the following equation:

$$\boldsymbol{\rho_{Cal.}} = [(\boldsymbol{wt_1}.\% \times \boldsymbol{\rho_1}) + (\boldsymbol{wt_2}.\% \times \boldsymbol{\rho_2}) + (\boldsymbol{wt_3}.\% \times \boldsymbol{\rho_3}) + \cdots]/\boldsymbol{100} \quad (2)$$

where $\boldsymbol{wt_{1,2\ and\ 3}}$ and $\boldsymbol{\rho_{1,\ 2\ and\ 3}}$ are the weight percent and densities of the alloy constituents.

While molar volume for the prepared samples was calculated according to the equation:

$$V_m = \sum_i^N (x_i\, M_i / \rho_{mixture}) \quad (3)$$

Where M_i is the molar mass of *i*-th alloys and ρ is the mixture density**.**

Table 1. Percentages of solutions for sample preparation.

Elements Wt.%	Steel Code					
	SS316L	SS316L W1	SS316L W2	SS316LTi	SS304L	SS304LTi
C	0.013	0.0369	0.044	0.031	0.016	0.036
Si	0.477	0.453	0.309	0.800	0.392	0.600
Mn	0.714	0.589	0.632	1.110	0.828	2.100
P	0.027	0.0269	0.0282	0.024	0.017	0.022
S	0.014	0.0138	0.0158	0.012	0.010	0.014
Cr	16.56	16.60	16.100	15.500	19.19	14.900
Ni	11.72	12.80	13.100	15.500	9.470	14.100
Mo	2.480	0.628	0.131	2.150	0.122	0.350
Al	0.004	0.001	0.001	0.011	0.001	0.045
Co	0.088	0.190	0.191	0.150	0.092	0.150
Cu	0.200	0.131	0.118	0.110	0.201	0.130
Nb	0.028	0.032	0.0314	0.030	0.027	0.030
Ti	0.002	0.002	0.0023	0.110	0.002	0.220
V	0.05	0.090	0.081	0.070	0.035	0.056
W	0.001	1.840	2.220	0.009	0.001	0.0150
Fe	67.622	66.46	66.99	64.383	69.596	67.232

2.5 Monte Carlo calculations

2.5.1 Gamma-ray measurements

MCNP5 (Monte Carlo N-Particle Transport Code version 5) is widely used for simulating the transport of particles, including gamma rays, through various materials. MCNP5 uses detailed photon interaction models, including photoelectric absorption, Compton scattering, and pair production, to simulate gamma-ray attenuation. The results from MCNP5 can be analyzed to calculate the mass attenuation coefficients based on the outputs and the geometry and material properties. The reference: X-5 Monte Carlo Team. (2003). MCNP—A General Monte Carlo N-Particle Transport Code, Version 5. Los Alamos National Laboratory, LA-UR-03-1987.
The mass attenuation coefficient is a quantity that describes the interaction probability between gamma photons and the mass per unit area for a certain medium and can be calculated by the well-known Beer-Lambert as follows:

$$\mu = \frac{ln(\frac{I_o}{I_\gamma})}{x} \quad (4)$$

$$HVL = \frac{ln2}{\mu} \quad (5)$$

Where, μ(cm^{-1}) is the linear attenuation coefficient of the sample, I and I_0 are the intensities of gamma rays after and before transmitted through the sample, and x is the thickness of the sample.

The theoretical attenuation coefficients were calculated for each sample composition based on the mixture rule of the following equation:

$$\sigma_{th.} = \sum_i^n W_i \left(\frac{\mu_i}{\rho_i}\right)_m \quad (6)$$

where, $\left(\frac{\mu_i}{\rho_i}\right)_m$ Is the mass attenuation coefficient for the individual element in each mixture sample, while W_i Is the fractional weight of the elements within each mixture.

2.5.2 Fast Neutron Cross section

Fast neutrons are produced by bombarding a target material with high-energy particles, such as protons or deuterons, using particle accelerators or other radiation-producing devices. The interaction of these high-energy particles with the target material induces nuclear reactions that release fast neutrons. Fast Neutrons have energies in the MeV range from about 0.5 to 11MeV. Accurate information about the geometry, detector-source distance, source dimensions, elemental and chemical composition, and densities of the stainless-steel samples under investigation (material card) must be included in the input file to perform a Monte Carlo simulation [18].

The neutron absorption cross-section for stainless steel can be determined using MCNP5 by defining the material composition, setting up a neutron source, and using tallies to measure the absorption reactions within the material.

$$\sum_{abs} = \boldsymbol{R_{abs}}/\emptyset \quad (7)$$

Where $\sum_{abs}$ Is the macroscopic absorption cross-section, R_{abs} is the reaction rate, and $\emptyset$ is the flux [19].

3 Results and Discussion

3.1 Thermodynamic calculations

The thermodynamic calculation was established by using the JMatPro database which is used for detecting the phases that can be formed. In SS316L intermetallic compounds appeared CHI and Laves as shown in Figure (1, a), while the addition of W in samples SS316LW1 and SS316LW2 caused a decreasing fraction of sigma phase, due to appearing stable carbides M23C6 at 900^{o}C and Laves phase appeared due to presence of W that did not appear in SS2, as shown in Figure (1, b and c). In SS316LTi, the Addition of Titanium causes the disappearance of the sigma phase and affects the stability of M23C6 and M (C, N) Carbides at high temperatures as shown in Figure (1, d). In SS304L Sigma phase appeared with a high fraction from 600 ^{o}C to 700 ^{o}C as shown in Figure (1, e) while in sample SS304LTi, the Addition of Ti caused the disappearance of the Sigma phase as shown in

Figure (1, f) Which will improve mechanical properties of the developed stainless-steel alloys as will be shown. From this result, it was found that stable carbides at high temperatures were formed which will affect positively to strength and mechanical properties, such as M23C6, of the prepared samples used as fuel cladding at high temperatures in nuclear reactors [20,21].

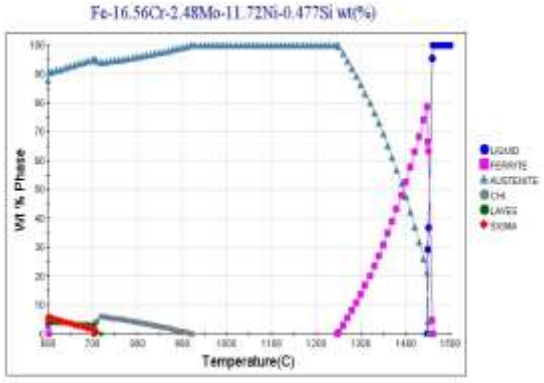

Fig. 1a. JMat Pro calculations for SS316L.

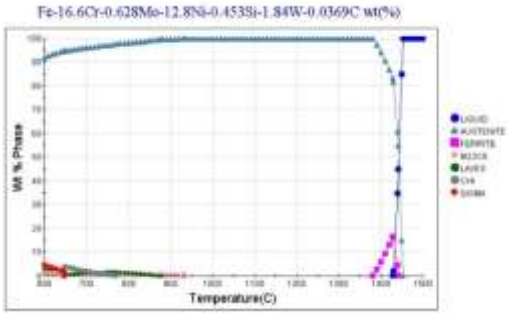

Fig. 1b. JMat Pro calculations for SS316LW1.

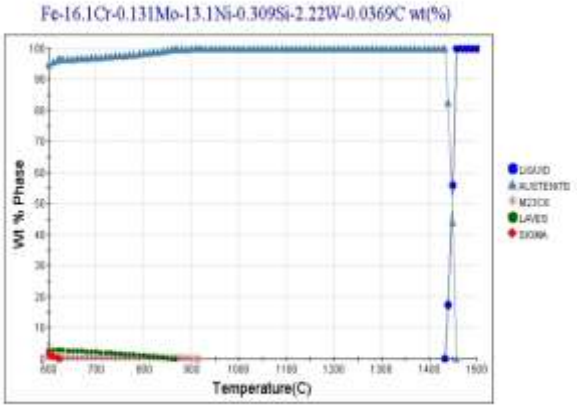

Fig.1c. JMat Pro calculations for SS316LW2.

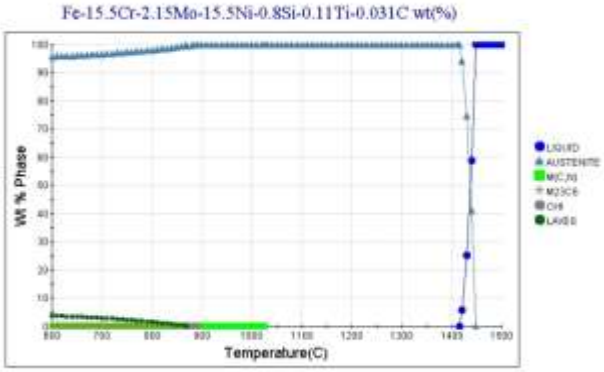

Fig. 1d. JMat Pro calculations for SS316LTi.

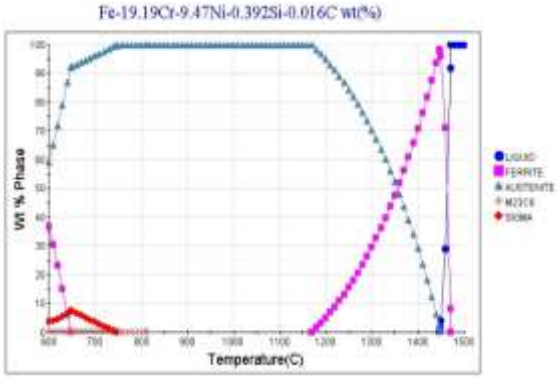

Fig. 1e. JMat Pro calculations for SS304L.

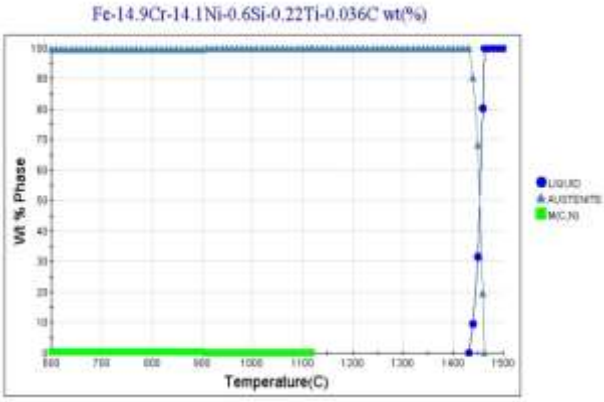

Fig. 1f. JMat Pro calculations for SS304LTi.

3.2 Microstructure Examinations

The optical micrographs of the studied samples are given in Figure (2). The investigation of these photos indicated that all samples have mainly austenite stainless steel structure, while in Figure (2, e) SS304L contains a large number of twins which characterize the appearance of the austenitic stainless steel. The addition of W has significantly changed the austenite grain size and retarding the growth of austenite grains.

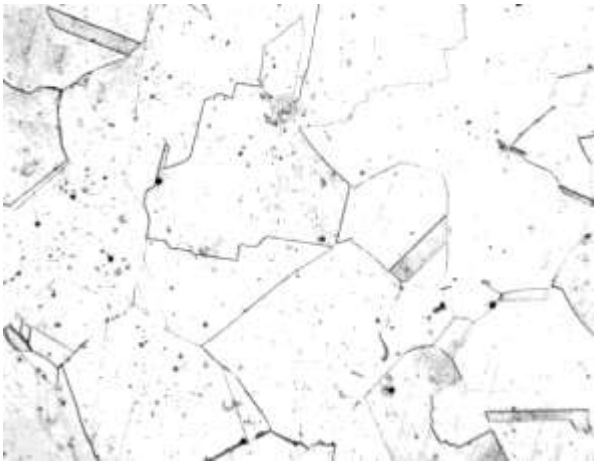

Fig. 2a. Microstructure for sample SS316L.

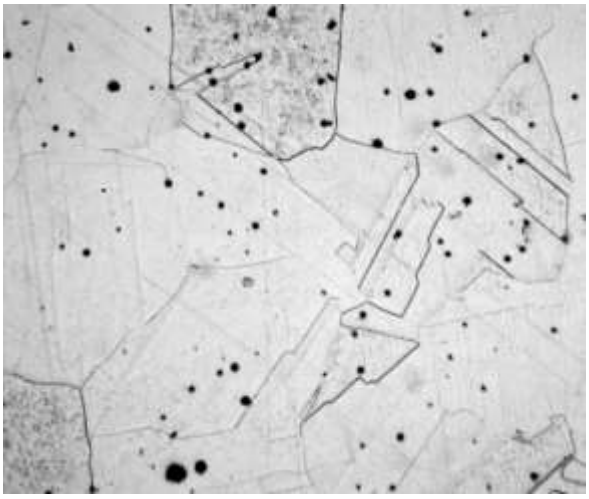

Fig. 2b. Microstructure for sample SS316LW1.

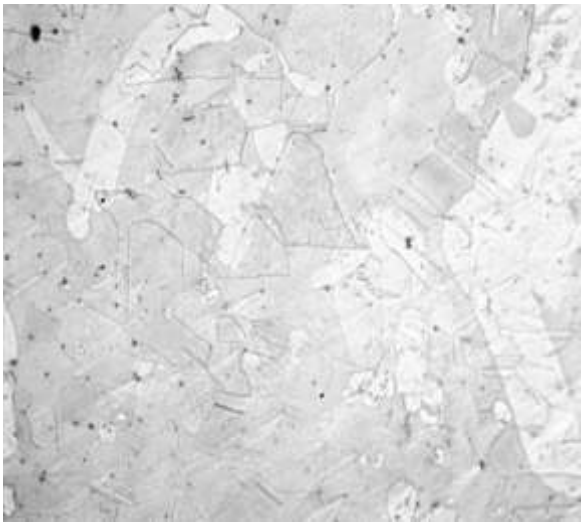

Fig. 2c. Microstructure for sample SS316LW2.

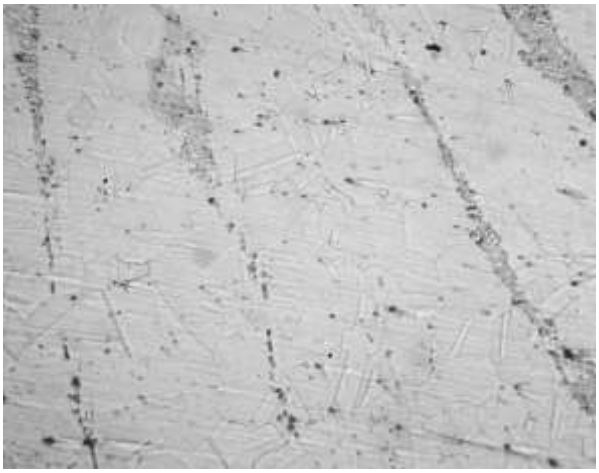

Fig. 2d. Microstructure for sample SS316LTi.

Fig. 2e. Microstructure for sample SS304L.

Fig. 2f. Microstructure for sample SS304LTi.

3.3 Mechanical properties

Table 2 contains the obtained results concerning the Ultimate Tensile Strength (MPa), Vickers Hardness (HV), and Yield Strength (MPa).

Hardness and impact energy results, it was found that hardness increased by either adding W to standard AISI316 or by increasing W percent as clarified in samples SS316LW1 and SS316LW2. The developed SS316LTi and SS304LTi steel alloy showed also higher hardness than the conventional stainless-steel alloys as shown in Figure (3). Both W and Ti are known to promote the formation of carbides, which can contribute to strengthening the material. Carbides act as obstacles to dislocation movement, making it harder for the material to deform. Consequently, the hardness of SS316L with W or Ti additions is generally higher compared to the base, as was expected from thermodynamic calculations [22-24].

Table 2. Physical and Mechanical properties of the prepared stainless-steel alloys.

Steel Code	Vickers Hardness (HV)	Yield Strength (MPa)	Ultimate Strength (MPa)
SS316L	224	270	544
SS316LW1	243	277	545
SS316LW2	256	300	587
SS316LTi	246	281	522
SS304L	175	296	625
SS304LTi	213	358	730

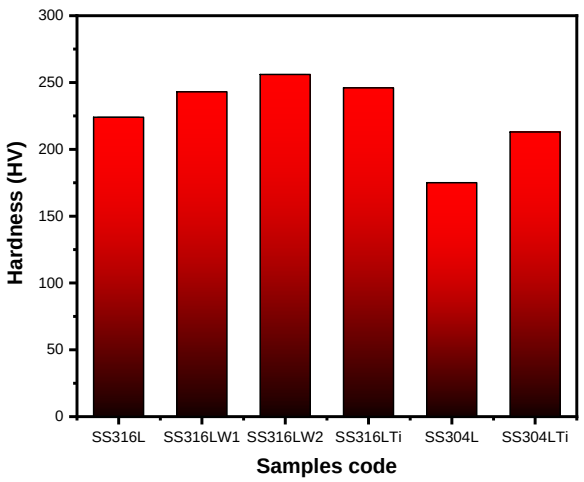

Fig. 3. Vickers hardness of the prepared stainless-steel alloys.

Figure (4) and Figure (5) show the relation between the prepared samples, yield strength, and Ultimate tensile strength of the investigated stainless-steel alloys, it was found that samples SS316LW1 and SS316LW2 much increment has been established in the yield strength is expected that this increment is due to the interaction between dislocations and fine intermetallic compounds based on tungsten [25, 26].

For samples SS316LTi and SS304lTi, titanium carbides caused a partial increment in toughness due to grain refinement caused by Ti. The addition of W and Ti to the samples improved the mechanical of the prepared samples that will be used as fuel cladding in nuclear reactors [27,28].

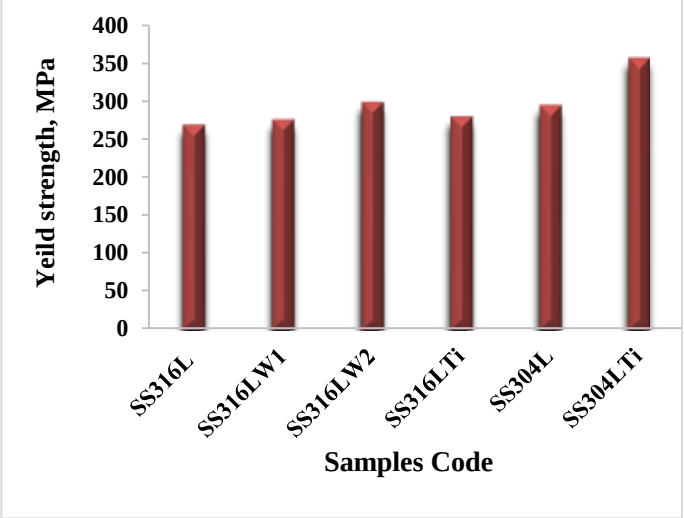

Fig. 4. Yield Strength for the investigated stainless-steel alloys.

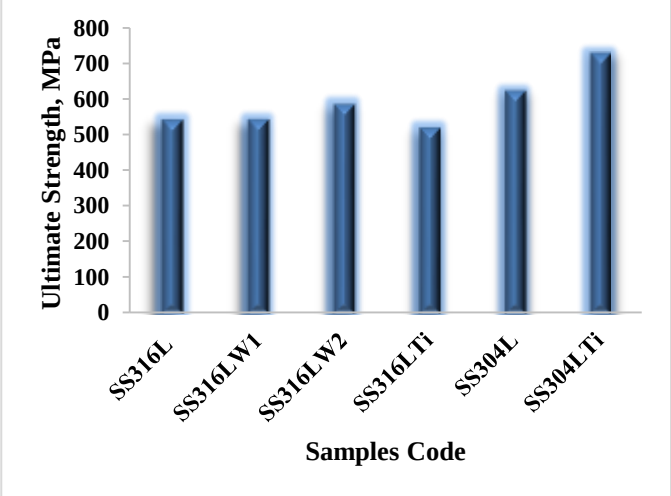

Fig. 5. Ultimate Tensile strength for the investigated stainless-steel alloys.

3.4 Density Measurements

The variations of both the experimental, calculated bulk densities and molar volume of the investigated stainless-

steel alloys are shown in Table 3. The experimental density for the prepared stainless-steel alloy agrees with the calculated density, which confirms the good agreement between the experimental and calculated densities of the prepared stainless-steel alloys. The densities of the modified stainless-steel alloys are greater than the standard alloy. SS316LW2 has the highest density among all prepared alloys and the lowest molar volume. Stainless steel alloy density plays a significant role in developing better radiation-shielding materials, the higher the stainless-steel density, the better the radiation-shielding effectiveness will be [29, 30].

Table 3: Density and molar volume of the prepared stainless-steel alloys.

Samples	Calc. Density g/cm^3	Exp. Density g/cm^3	Molar Volume cm^3/mole	Porosity %
SS316L	7.903	7.790±0.028	7.137	0.014
SS316LW1	8.092	7.989±0.002	7.165	0.013
SS316LW2	8.126	8.054±0.010	7.186	0.009
SS316LTi	7.919	7.863±0.051	7.111	0.007
SS304L	7.811	7.634±0.058	7.082	0.023
SS304LTi	7.868	7.773±0.016	7.068	0.012

3.5 Gamma-ray measurements

The linear attenuation coefficient of the prepared stainless-steel alloys is listed in Table (4). The observed behavior in mass attenuation coefficients as shown in Figure (6), could be explained by photon energy and Z-dependency of interaction cross-section of the elements. Two different regions were observed in the behavior of mass attenuation coefficients. First region, there is a sharp decrease of mass attenuation coefficients in the energy range from 121.8 keV up to 661.64 keV because the dominant reaction between the investigated stainless-steel samples and gamma rays is the photoelectric effect. Secondly, a slight decrease in mass attenuation coefficients was observed from 661.64 keV up to 1407.24 keV which was attributed to the Compton scattering process. The comparison of half-value layers of different types of investigated steel alloys for different investigated gamma-ray energies is shown in Table (5). The half-value layer has great significance due to its indication in thickness value, the lower the HVL value, the higher the effectiveness of shielding material at the related photon energy [31, 32].

Table 4: Linear attenuation coefficient of the prepared stainless-steel alloys.

Eγ MeV	Linear attenuation coefficient, cm^{-1}					
	SS316L	SS316LW1	SS316LW2	SS316LTi	SS304L	SS304LTi
0.1218	7.36567	7.541663	7.580908	7.389536	6.96491	7.147134
0.34427	0.810137	0.829349	0.868832	0.848442	0.775476	0.782709
0.662	0.58174	0.59549	0.603112	0.58949	0.570047	0.57578
0.7789	0.55645	0.569596	0.578734	0.565733	0.540365	0.549816
0.964	0.494807	0.506478	0.518601	0.507133	0.48725	0.491593
1.1124	0.475761	0.486977	0.495767	0.48488	0.467254	0.473103
1.17323	0.434744	0.444979	0.451156	0.441405	0.428668	0.432583
1.33251	0.416567	0.426367	0.434091	0.424775	0.40914	0.412913
1.40724	0.413643	0.423373	0.427346	0.416935	0.408437	0.411496

Table 5: Half-value layer of the prepared stainless-steel alloys.

Eγ MeV	Half value layer HVL, cm					
	SS316L	SS316LW1	SS316LW2	SS316LTi	SS304L	SS304LTi
0.1218	0.094112	0.091916	0.09144	0.093808	0.099527	0.09699
0.34427	0.855658	0.835836	0.797853	0.817027	0.893902	0.885642
0.662	1.191598	1.164083	1.149372	1.175931	1.216041	1.203932
0.7789	1.245754	1.217003	1.197787	1.225312	1.282837	1.260786
0.964	1.400951	1.368667	1.336672	1.3669	1.422678	1.410111
1.1124	1.457035	1.423477	1.398237	1.429631	1.483561	1.465221
1.17323	1.594501	1.557826	1.536499	1.57044	1.617103	1.602468
1.33251	1.664078	1.625828	1.5969	1.631922	1.694285	1.678805
1.40724	1.675841	1.637325	1.622104	1.662608	1.697201	1.684583

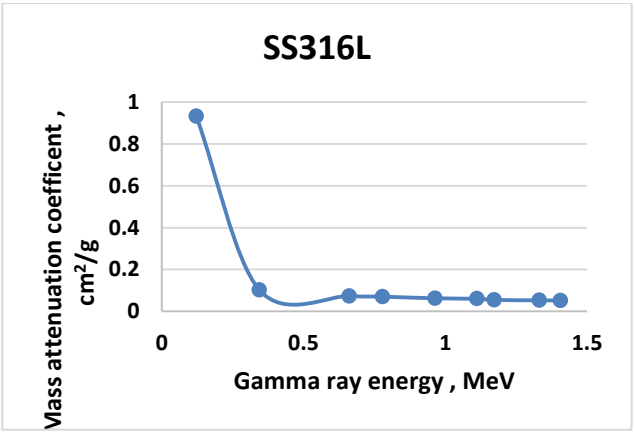

Fig. 6a: Mass attenuation coefficients for SS316L stainless-steel alloys.

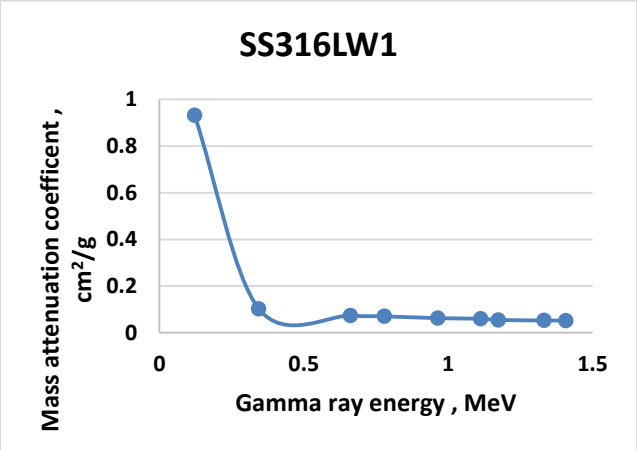

Fig.6b: Mass attenuation coefficients for SS316LW1 stainless-steel alloys.

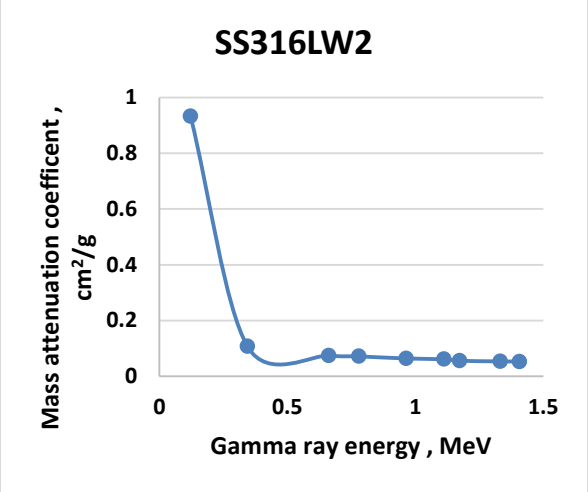

Fig. 6c: Mass attenuation coefficients for SS316LW2 stainless-steel alloy.

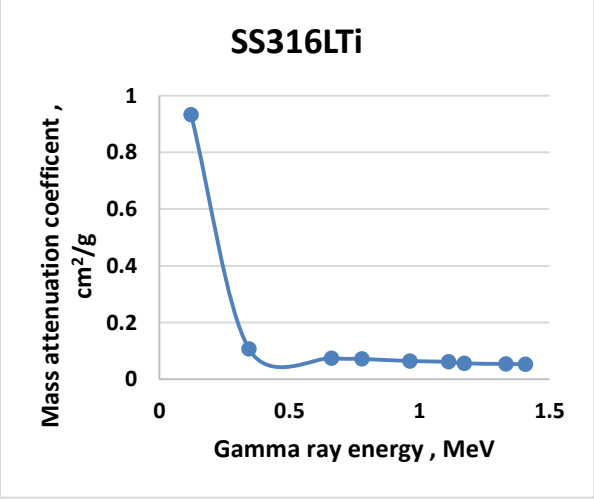

Fig.6d: Mass attenuation coefficients for SS316LTi stainless-steel alloy.

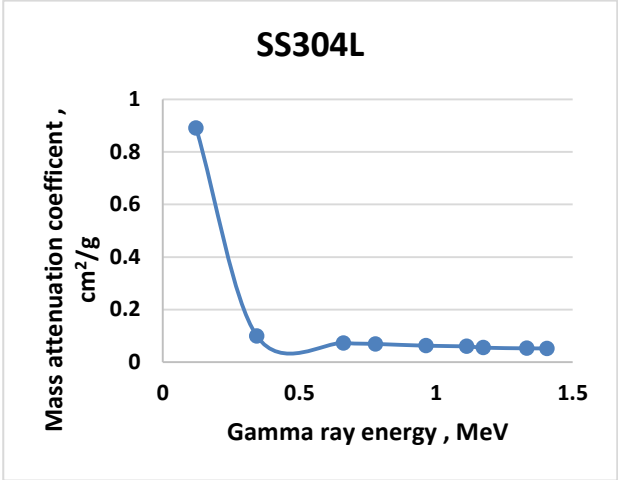

Fig. 6e: Mass attenuation coefficients for SS304L stainless-steel alloy.

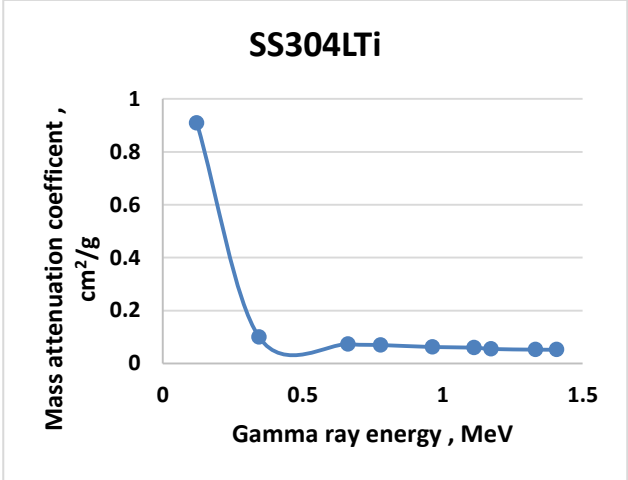

Fig.6f: Mass attenuation coefficients for SS304LTi stainless-steel alloys.

3.6 Neutrons measurements

Fast Neutrons have energies in the MeV range from about 0.5 to 11MeV. The outer diameter of the cladding is 7.4 mm and the cladding thickness is 0.5mm which was used to calculate the neutron cross section in the program [33].

The total cross-section and absorption cross-section of fast neutrons were calculated using the MNCP5. As shown in Figure (7), the total neutron cross-section of SS316L decreased with the addition of tungsten in SS316LW1 and SS316LW2, while the addition of titanium increased the total neutron cross-section owing to (n, n') reaction of fast neutrons with Fe and MO. The total neutron cross-section of SS304LTi is lower than SS304L due to the addition of titanium to the sample. It is also observed that the absorption

neutron cross section of neutrons shown in Figure (8) that, SS316LW1 has the lower absorption cross section so it will be a good candidate as a fuel cladding in fast nuclear reactor that will not absorb the neutron from the reactor core and the self-sustained chain reaction will be continuous. SS304L and SS304LTi have the highest absorption cross section that could be used in the reactor structural material. Furthermore, Figure (9) shows the mean free path, MFP, for all investigated samples that reported that SS316LW1 has the lowest mean free path, these results demonstrate that the average distance between subsequent collisions in the studied alloys is relatively small.

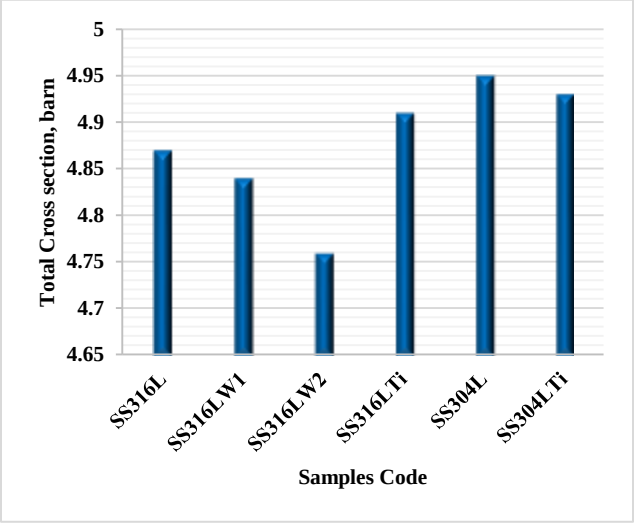

Fig. 7: Total neutron cross-section of the investigated stainless-steel alloys.

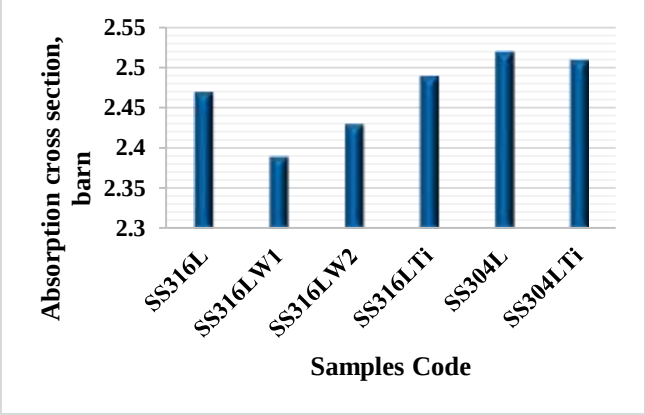

Fig. 8: Absorption neutron cross-section of the investigated stainless-steel alloys.

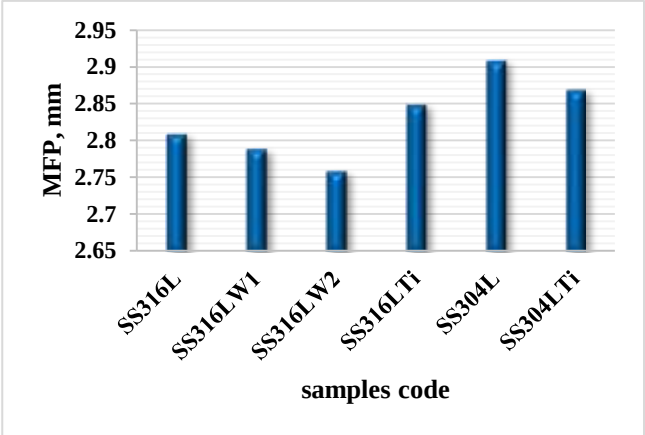

Fig. 9: Mean free path, MFP of the investigated stainless-steel alloys.

4 Conclusions

To develop stainless steel alloys suitable to be used as fuel cladding in fast breeder reactors, six steel alloys were prepared. The first two samples (SS316L) and (SS304L) conform the chemical composition of standard AISI 316L and AISI 304L respectively, and two alloys were prepared by partial and full replacement of Mo by W to the standard SS316L, while the other two alloys were developed by modification of Cr, Ni and micro-alloyed with titanium to the standard alloys SS316L and SS304L. The structural, mechanical, and nuclear properties of the prepared steels are investigated. From the results obtained, the following conclusions are drawn:

1. Tungsten has a high affinity for forming intermetallic compounds like CHI and laves phases which positively on strength and hardness of the investigated stainless-steel alloys.
2. There is a great refinement in austenite structure attributed to Ti- microalloying, causing higher strength and very significant enhancement in impact energy.
3. Both tungsten and titanium cause the disappearance of the sigma phase and promote the formation of carbides, which can contribute to strengthening the material making it harder for the material to deform.
4. The hardness and strength of the developed stainless-steel alloys are generally higher compared to the conventional SS316L and SS304L.
5. The density of modified stainless-steel alloys is greater than the standard alloy so, the higher the stainless-steel density, the better the effectiveness of the radiation shielding.

6. SS316LW2 sample has the lowest HVL the higher the effectiveness of shielding material at the related photon energy.
7. Absorption neutron cross-sections of SS316LW1 SS316LW2 stainless-steel alloys are lower than the other types of stainless-steel alloys investigated and SS316LW2 has the lowest values of MFP in all types of neutron energies.
8. The developed SS316LW2 exhibits the highest hardness, strength, and microscopic cross-sections among the investigated steel alloys.

References

[1] Sun, C., S. Zheng, C. C. Wei, Y. Wu, L. Shao, Y. Yang, K. T. Hartwig, et al. "Superior radiation-resistant nanoengineered austenitic 304L stainless steel for applications in extreme radiation environments." Scientific Reports., **5(1)**, 7801, 2015.

[2] Eissa, M. M., S. U. El-Kameesy, S. A. El-Fiki, S. N. Ghali, R. M. El Shazly, and Aly Saeed. "Attenuation capability of low activation-modified high manganese austenitic stainless steel for fusion reactor system." Fusion Engineering and Design., **112**, 130-135, 2016.

[3] Murty, K. Linga, and Indrajit Charit. "Structural materials for Gen-IV nuclear reactors: Challenges and opportunities." Journal of nuclear materials., **383(1-2)** 189-195, 2008.

[4] Allen, Todd R., Jeremy T. Busby, Ronald L. Klueh, Stuart A. Maloy, and Mychailo B. Toloczko. "Cladding and duct materials for advanced nuclear recycle reactors." Jom 60, 15-23, 2008.

[5] Hoffman, E. A., R. N. Hill, and T. A. Taiwo. "Estimated cost for low conversion ratio burners." Transactions of the American Nuclear Society., **91**, 768-769, 2008.

[6] Duan, Zhengang, Huilong Yang, Yuhki Satoh, Kenta Murakami, Sho Kano, Zishou Zhao, Jingjie Shen, and Hiroaki Abe. "Current status of materials development of nuclear fuel cladding tubes for light water reactors." Nuclear Engineering and Design., **316**, 131-150, 2017.

[7] Singh, Vishwanath P., M. E. Medhat, and S. P. Shirmardi. "Comparative studies on shielding properties of some steel alloys using Geant4, MCNP, WinXCOM, and experimental results." Radiation Physics and Chemistry., **106**, 255-260, 2015.

[8] S. U. El-Khameesy, M. M. Eissa, S. A. El-Fiki, R. M. El Shazly, S. N. Ghali, Aly Saeed, "The Attenuation Capability of Selected Steel Alloys for Nuclear Reactor Applications", Journal of Advances in Physics., **11**, 3139-3145, 2016.

[9] Series, IAEA Nuclear Energy. "Structural Materials for Liquid Metal Cooled Fast Reactor Fuel Assemblies–Operational Behaviour." International Atomic Energy Agency (IAEA), Vienna, Austria, Report No. NF (2012).

[10] Aygün, Bünyamin. "High alloyed new stainless steel shielding material for gamma and fast neutron radiation." Nuclear Engineering and Technology., **52(3)**, 647-653, 2020.

[11] Karthik, V., S. Murugan, P. Parameswaran, C. N. Venkiteswaran, K. A. Gopal, N. G. Muralidharan, S. Saroja, and K. V. Kasiviswanathan. "Austenitic stainless steels for fast reactors-irradiation experiments, property evaluation and microstructural studies." Energy Procedia., 7, 257-263, 2011.

[12] Min, Ki-Deuk, Seokmin Hong, Dae-Whan Kim, Bong-Sang Lee, and Seon-Jin Kim. "Fatigue crack growth characteristics of nitrogen-alloyed type 347 stainless steel under operating conditions of a pressurized water reactor." Nuclear Engineering and Technology., **49(4)**,752-759, 2017.

[13] Prifiharni, Siska, Moch Syaiful Anwar, Arini Nikitasari, and Efendi Mabruri. "The hardness, microstructure, and pitting resistance of austenitic stainless steel Fe25Ni15Cr with the addition of tungsten, niobium, and vanadium." In AIP Conference Proceedings., **1964(1)**, 020041, 2018.

[14] Zhao, Jingwei, Taekyung Lee, Jeong Hun Lee, Zhengyi Jiang, and Chong Soo Lee. "Effects of tungsten addition on the microstructure and mechanical properties of micro-alloyed forging steels." Metallurgical and Materials Transactions., **A 44**, 3511-3523, 2013.

[15] Salama, E., M. M. Eissa, and A. S. Tageldin. "Distinct properties of tungsten austenitic stainless alloy as a potential nuclear engineering material." Nuclear Engineering and Technology., **51(3)**, 784-791,2019.

[16] Haugan, Eirik B., Monika Næss, Cristian Torres Rodriguez, Roy Johnsen, and Mariano Iannuzzi. "Effect of tungsten on the pitting and crevice corrosion resistance of type 25Cr super duplex stainless steels." Corrosion., **73(1)**, 53-67, 2107.

[17] Higuchi, J. I., and Eiki Nagashima. "Development Of DP28 W™ duplex stainless." Stainless Steel World., 29-32, 2009.

[18] Rehab M El-Sharkawy, Elhassan A Allam, Atef El-Taher, Reda Elsaman, E El Sayed Massoud, Mohamed E Mahmoud, Synergistic effects on gamma-ray shielding by novel light-weight nanocomposite materials of bentonite containing nano Bi2O3 additive. Ceramics International., **48(5)**, 7291-7303.2022

[19] El-Sharkawy, R., Allam, EA ., El-Taher, A., Shaaban,

ER and Mahmoud, ME., Synergistic effect of nano-bentonite and nanocadmium oxide doping concentrations on assembly, characterization, and enhanced gamma-rays shielding properties of polypropylene. International Journal of Energy Research., **45(6**), 8942-8959, 2021

[20] Maher, Majdouline, Itziar Iraola-Arregui, Hicham Ben Youcef, Benaissa Rhouta, and Vera Trabadelo. "Microstructural evolution of heat-treated Cr–W–V–Mo steels: effect of core-shell carbides and secondary precipitation on their abrasion resistance." Journal of Materials Research and Technology., **24**,27-38, 2023.

[21] Garbade, R. R., and N. B. Dhokey. "Effect of mechanical alloying of Ti and B in pre-alloyed gas atomized powder on carbide dispersed austenitic matrix of Iron-based hard-facing alloy." Materials Characterization., **191**,112134, 2022.

[22] Kaddour, Houria, Fatah Hellal, Ahmed Haddad, and Zoheir Boutaghou. "Effect of the Coarsening of Austenite Grain on the Microstructure and Corrosion Behavior of a Cold Rolled AISI 316Ti Stainless Steel." Int. J. Electrochem. Sci 17(220749),2, 2022.

[23] Wu, Mingyu, Ke Chen, Zhen Xu, and D. Y. Li. "Effect of Ti addition on the sliding wear behavior of AlCrFeCoNi high-entropy alloy." Wear 462,203493, 2020.

[24] Özbek, Nursel Altan, Adem Çiçek, Mahmut Gülesin, and Onur Özbek. "Effect of cutting conditions on wear performance of cryogenically treated tungsten carbide inserts in dry turning of stainless steel." Tribology International **94**, 223-233, 2016.

[25] Yin, Xiaotian, Qiang Zhai, Qingxia Zhang, Kunlun Wang, Lingtao Meng, Zhenghang Ma, Guoxia Chen, Shenghai Wang, and Li Wang. "Effect of tungsten particles on microstructure and properties of 316 L stainless steel manufactured by selective laser melting." Journal of Manufacturing Processes **68**,210-221, 2021.

[26] Han, Soo Bin, Yoon Sun Lee, Sung Hyuk Park, and Hyejin Song. "Ti-containing 316L stainless steels with excellent tensile properties fabricated by directed energy deposition additive manufacturing." Materials Science and Engineering: A 862 (2023): 144414.

[27] Piekarski, Bogdan. "Effect of Nb and Ti additions on microstructure, and identification of precipitates in stabilized Ni-Cr cast austenitic steels." Materials characterization., **47(3-4)**,181-186, 2011.

[28] Sadeghpour, S., A. Kermanpur, and A. Najafizadeh. "Influence of Ti microalloying on the formation of nanocrystalline structure in the 201L austenitic stainless steel during martensite thermomechanical treatment." Materials Science and Engineering., **A 584**,177-183, 2013.

[29] Rilwan, U ., Aliyu, GM ., Olukotun, SF., Idris, MM., Mundi, AA., Bello, S., Umar, I., El-Taher, A. and Mahmoud, KA.., Recycling and characterization of bone incorporated with concrete for gamma-radiation shielding applications. Nuclear Engineering and Technology., **56(7)**, 2828-2834.2024.

[30] Raut, A. P., and V. K. Deshpande. "Influence of alumina addition and gamma irradiation on the lithium borosilicate glasses." Radiation Physics and Chemistry., **149**,118-125, 2018.

[31] Rilwan, U ., Edeh, SA ., Idris, MM., Fatima, II., Olukotun, SF., Arinseh, GZ ., Bonat, PZ., El-Taher, A., Mahmoud, KA., Taha A Hanafy, MI Sayyed., Influence of waste glass on the gamma-ray shielding performance of concrete. Annals of Nuclear Energy., **210**, 110876. 2025.

[32] Elhassan A Allam, Rehab M El-Sharkawy, Atef El-Taher, ER Shaaban, E El Sayed Massoud, Mohamed E Mahmoud., Enhancement and optimization of gamma radiation shielding by doped nano HgO into nanoscale bentonite. Nuclear Engineering and Technology., **54 (6)**, 2253-2261.2022.

[33] Lee, Chan Bock, Jin Sik Cheon, Sung Ho Kim, Jeong-Yong Park, and Hyung-Kook Joo. "Metal fuel development and verification for prototype generation IV sodium-cooled fast reactor." Nuclear Engineering and Technology., **48(5)**,1096-1108, 2016.